Air Gap and Edge Effect in the 2-D/1-D Method With the Magnetic Vector Potential *A* Using MSFEM

Karl Hollaus and Markus Schöbinger

Institute for Analysis and Scientific Computing, Technische Universität Wien, 1040 Vienna, Austria.

Eddy currents (ECs) are simulated in a single laminate, representing the whole core of an electrical machine. Despite this drastic reduction in the complexity of the problem, a 3-D finite-element model turns out to be still too expensive for simulations. To overcome this difficulty, 2-D/1-D methods are used. This article presents a solution to consider both air gap and edge effect (EE) based on the multiscale finite-element method (MSFEM) using the magnetic vector potential (MVP) *A*. Linear material properties are assumed; therefore, this article is carried out in the frequency domain. The new 2-D/1-D MSFEM is discussed, and various simulation results are presented.

***Index Terms*— 2-D/1-D method, eddy-current (EC) problems, edge effect (EE), iron core, lamination, magnetic vector potential (MVP) *A*, multiscale finite-element method (MSFEM).**

I. Introduction

EFFICIENT simulations of eddy currents (ECs) in laminated cores with the finite-element method (FEM) are of great interest in the design of electrical machines. The scales of the geometric dimensions are extremely different, compared with Fig. 1. The overall dimensions, the radii R and r and the length L, are in the range of meters, whereas the thickness d of the laminates and the air gaps d_0 in between are the fractions of millimeters. Many finite elements are required for an accurate model, resulting in extremely large equation systems that are impossible to solve reasonably. However, a laminated core represents a quasi-periodic structure with the period $p = d + d_0$ and is thus well suited for the multiscale FEM (MSFEM).

A simple laminate is shown in Fig. 2. In general, there is a magnetic stray field $\boldsymbol{B}_s$ penetrating the plane of the laminate perpendicularly, inducing large EC loops $\boldsymbol{J}_s$ on the one hand and the main magnetic field $\boldsymbol{B}_m$ on the other, which is parallel to the plane of the laminate and causes ECs $\boldsymbol{J}_m$ confined to flow in narrow loops. The ECs $\boldsymbol{J}_m$ consist of a laminar part, i.e., currents are flowing parallel to the plane of the laminate, and a part that is perpendicular to the plane, representing the edge effect (EE). It is very common to neglect the magnetic stray fields in the end region and, therefore, reasonable to assume that all laminates are exposed to the same electromagnetic-field distribution. Thus, it suffices to simulate only one single laminate instead of the whole laminated core.

Brute force 3-D standard FEM (SFEM) models are still too expensive [1] for routine simulations. To avoid them, the problem is solved using the ideas of the MSFEM [2] and the 2-D/1-D methods [3], [4], which are very efficient for this specific purpose. A significant shortcoming of these methods based on the magnetic vector potential (MVP) $\boldsymbol{A}$ is the inability to consider air gaps and the EE [5], [6]. Using a 2-D/1-D MSFEM based on a current vector potential considers the EE just by imposing appropriate boundary conditions [7].

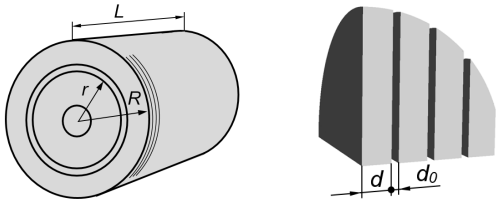

Fig. 1. Large scale: electrical machine with overall dimensions L, R, and r; lamination is indicated (left). Fine scale: thickness d of the laminates and the width d_0 of the air gaps or the insulation (right).

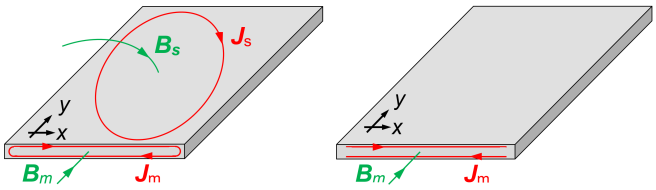

Fig. 2. Magnetic fields and ECs in general associated with a laminate (left), without stray field $\boldsymbol{B}_s$ and currents $\boldsymbol{J}_s$ and without EE (right).

The EE is of great importance in the simulations of narrow ferromagnetic strips [8] for material degradation due to punching [9] and so on. The inclusion of an air gap can easily be substantiated. The overall dimensions of the electrical machines include the air gaps. Neglecting the air gaps leads to essentially higher losses for the same total magnetic flux.

The new 2-D/1-D method with the MVP copes with both the EE and an air gap and performs excellently. Therefore, it is a very attractive alternative to brute force 3-D SFEMs.

II. Multiscale Finite-Element Method

A suitable selection of the local basis is essential for a well-performing MSFEM [10]. Only odd polynomials are relevant, since the MVP is odd versus z: Gauss–Lobatto

Manuscript received November 11, 2018; revised October 4, 2019; accepted October 16, 2019. Date of current version December 20, 2019. Corresponding author: K. Hollaus (e-mail: karl.hollaus@tuwien.ac.at).

Color versions of one or more of the figures in this article are available online at http://ieeexplore.ieee.org.

Digital Object Identifier 10.1109/TMAG.2019.2949004

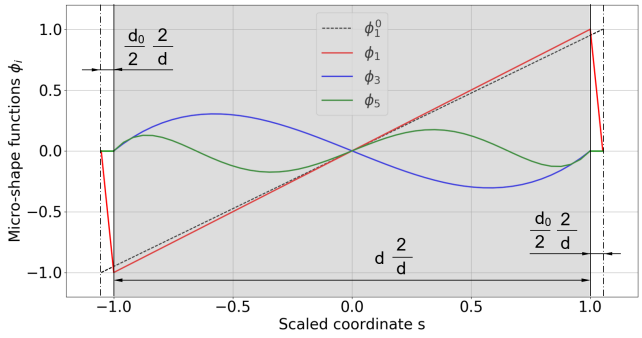

Fig. 3. MSFs: the gray interval $[-1, 1]$ represents the iron laminate, and beyond that up to the dashed–dotted line, there is the air gap.

polynomials

$$\phi_1(s) = s, \quad \phi_3(s) = \frac{1}{2}\sqrt{\frac{5}{2}}(s^2-1)s$$
$$\phi_5(s) = \frac{1}{8}\sqrt{\frac{9}{2}}(s^2-1)(7s^2-3)s, \ldots \tag{1}$$

are used as micro-shape functions (MSFs) ϕ_i with the mapping $s = 2z/d$, where $s \in [-1, 1]$ and $z \in [-d/2, d/2]$. Fig. 3 shows how the MSFs fit into the periodic structure with p. They are extended by zero in $[-(d + d_0)/2, -d/2]$ and $[d/2, (d + d_0)/2]$ including the air gap, except ϕ_1^0 and ϕ_1, which are extended linearly and become ± 1 and 0 in $\{-(d + d_0)/2, (d + d_0)/2\}$, respectively (see Fig. 3). These polynomials facilitate the required tangential continuity of the unknown MVP, and ϕ_1^0 allows to prescribe essential boundary conditions.

III. 2-D/1-D Method With A Based on MSFEM

The idea is to write the 2-D/1-D MSFEM approach $\tilde{\boldsymbol{u}}$ as a truncated sum

$$\tilde{\boldsymbol{u}}(x, y, z) \approx \sum_i L_i \phi_i(z) \boldsymbol{u}_i(x, y) \tag{2}$$

based on the space splitting $\Omega = \Omega_{2D} \times [-(d + d_0)/2, (d + d_0)/2]$, where the values of L_i are the linear differential operators, either the gradient or the identity, and the values of $\boldsymbol{u}_i(x, y)$ are the unknown functions. The tilde marks the multiscale approach. The approach (2) has two advantages compared with 3-D-FEMs, namely, that the unknown functions $\boldsymbol{u}_i$ depend solely on x and y, which means a weaker coupling between the unknowns, and it assumes only odd polynomials in z.

A. Old 2-D/1-D MSFEM Approach

Our original approach

$$\tilde{\boldsymbol{A}} = \phi_1(z)\,\mathrm{grad}(u_1(x, y)) + \phi_3(z)\boldsymbol{A}_3(x, y) + \phi_5(z)\boldsymbol{A}_5(x, y) + \cdots \tag{3}$$

with $u_1 \in H^1(\Omega_{2D})$ and $\boldsymbol{A}_3, \boldsymbol{A}_5, \ldots \in H(\mathrm{curl}, \Omega_{2D})$ considered neither an air gap nor the EE (see Fig. 4). The third- and fifth-order terms in (3) represent the higher order approach, and ϕ_1 is restricted to iron.

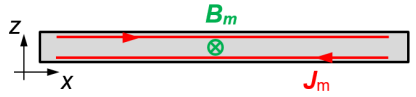

Fig. 4. Single laminate with ECs without EE, main magnetic field B_m, and currents J_m.

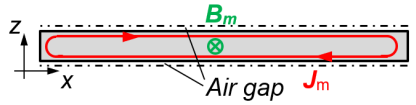

Fig. 5. Single laminate with ECs with EE and air gap, main magnetic field B_m, and associated currents J_m.

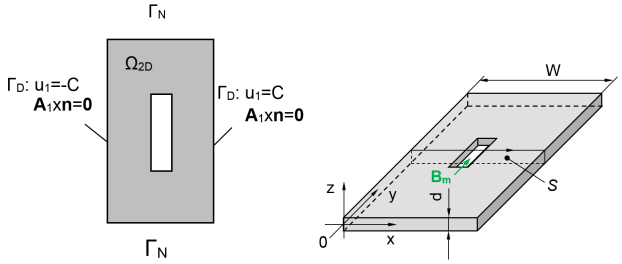

Fig. 6. Boundary conditions for u_1 and $\boldsymbol{A}_1$, representing a flux tube.

B. New 2-D/1-D MSFEM Approach

The new linear 2-D/1-D MSFEM approach

$$\tilde{\boldsymbol{A}} = \phi_1^0(z)\,\mathrm{grad}(u_1(x, y)) + \phi_1(z)\boldsymbol{A}_1(x, y) + \mathrm{grad}(\phi_1(z)w_1(x, y)) \tag{4}$$

with $\boldsymbol{A}_1 \in H(\mathrm{curl}, \Omega_{2D})$ and $u_1, w_1 \in H^1(\Omega_{2D})$ uses two different linear MSFs, ϕ_1 and ϕ_1^0, which are shown in Fig. 3. The support for both functions is iron and air. The first term in (4) prescribes a total magnetic flux, and the second term splits the total magnetic flux into one flowing in the iron and one in the air gap, respectively, and corrects the laminar currents according to the magnetic flux in the iron, compared with Fig. 5. The third term considers the EE. Due to the selection of both linear MSFs, ϕ_1^0 and ϕ_1, respectively, the introduction of the third term becomes feasible (see Table I).

1) Excitation, Boundary Conditions: A total magnetic flux Φ through the cross section S in Fig. 6 can be prescribed by

$$\begin{aligned}\Phi &= \int_S \boldsymbol{B}_m \cdot \boldsymbol{e}_y\, dS = \int_S \mathrm{curl}\,\tilde{\boldsymbol{A}} \cdot \boldsymbol{e}_y\, dS \\ &= \int_S \mathrm{curl}\left(\phi_1^0(z)\,\mathrm{grad}(u_1(x, y)) + \phi_1(z)\boldsymbol{A}_1(x, y)\right) \cdot \boldsymbol{e}_y\, dS \\ &= \int_{-\frac{d+d_0}{2}}^{\frac{d+d_0}{2}} \phi_{1,z}^0\, dz \int_0^w u_{1,x}\, dx = 2(u_1(w, y) - u_1(0, y)) = 2C.\end{aligned} \tag{5}$$

Planes of symmetry are discussed in Section IV-A2.

2) Weak Form of the 2-D/1-D MSFEM: An EC problem in the frequency domain has to be solved using the phasor convention $e^{j\omega t}$. To obtain the weak form of the new 2-D/1-D MSFEM, the approach (4) represents the trial function, and

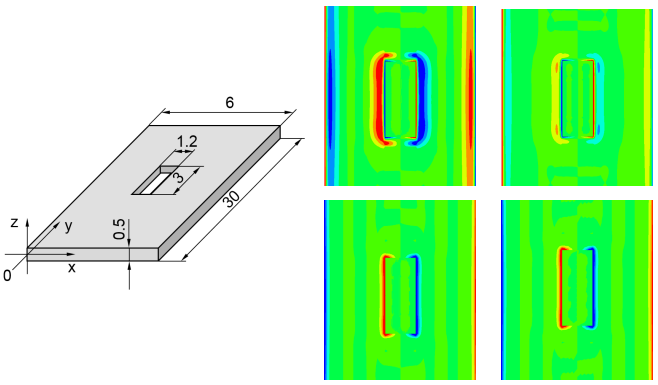

Fig. 7. Laminate with a hole, $\Omega_{2D} = [0, 6] \times [0, 30]$; dimensions in mm (left). Current densities in the vicinity of the hole in the plane of symmetry at $z = 0.0$—3-D SFEM (middle) and 2-D/1-D MSFEM with EE (right): z-components $\mathrm{Re}\{\boldsymbol{J}_z\}$ (above, ± 0.15 MA/m^2) and $\mathrm{Im}\{\boldsymbol{J}_z\}$ (below, ± 2.0 MA/m^2), $f = 1000$ Hz.

according to the Galerkin method, the test function

$$\tilde{\boldsymbol{v}} = \phi_1^0(z)\,\mathrm{grad}(v_1(x, y)) + \phi_1(z)\boldsymbol{v}_1(x, y) + \mathrm{grad}(q_1(x, y)\phi_1(z)) \quad (6)$$

is selected. The weak form reads as follows.

Find $(u_{1h}, \boldsymbol{A}_{1h}, w_{1h}) \in V_C := \{(u_{1h}, \boldsymbol{A}_{1h}, w_{1h}) : u_{1h}, w_{1h} \in \mathcal{U}_h, \boldsymbol{A}_{1h} \in \mathcal{V}_h, u_{1h} = \pm C \text{ and } \boldsymbol{A}_{1h} \times \boldsymbol{n} = \boldsymbol{0} \text{ on } \Gamma_D\}$, such that

$$\int_\Omega \mu^{-1}\,\mathrm{curl}(\tilde{\boldsymbol{A}}) \cdot \mathrm{curl}(\tilde{\boldsymbol{v}})\,d\Omega + j\omega \int_\Omega \sigma\,\tilde{\boldsymbol{A}} \cdot \tilde{\boldsymbol{v}}\,d\Omega = 0 \quad (7)$$

for all $(v_{1h}, \boldsymbol{v}_{1h}, q_{1h}) \in V_0$.

We propose using the finite-element subspaces $\mathcal{U}_h \subset H^1(\Omega_{2D})$ and $\mathcal{V}_h \subset H(\mathrm{curl}, \Omega_{2D})$, respectively. The MSFs ϕ_i (except ϕ_1^0) are in the space of continuous and periodic functions $H_{\mathrm{per}}(\Omega)$.

Essential boundary conditions are prescribed on $\Gamma_D \subset \partial\Omega_{2D}$.

Since the problem is linear and due to the space-splitting approach, integrations in (7) over $[-(d + d_0)/2, (d + d_0)/2]$ are carried out analytically. For averaging of the coefficients, which are involved in (7), see [2].

IV. Numerical Example

The laminate in Fig. 7 with a hole arranged symmetrically in the center has been chosen to study in particular the EE. The material parameters $\sigma = 2.08 \times 10^6$ S/m and $\mu = 1000\ \mu_0$ have been selected. Boundary conditions are prescribed such that a total flux Φ flows into the y-direction.

A. Results

Results obtained by the 2-D/1-D MSFEMs are compared with reference solutions computed with the 3-D SFEM using the mixed formulation $\boldsymbol{A}, V - \boldsymbol{A}$ to prescribe suitable boundary conditions.

The number of degrees of freedom (NDOF) and EC losses are summarized in Table I. The computational costs are reduced by the 2-D/1-D MSFEM compared with the 3-D SFEM by a factor of about 16. The new MSFEM is very accurate.

TABLE I
EC Losses at $f = 100$ Hz

FE model	NDOF H^1 of 3^{rd} order	NDOF $H(curl)$ of 2^{nd} order	Losses μW
3D SFEM		305,203	709
Old [a])	4,675	9,210	718
New [b])	9,350	9,210	712
Wrong [c])	9,350		$115 \cdot 10^3$

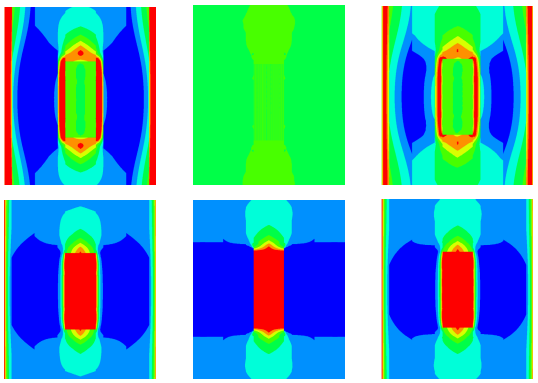

Fig. 8. Current densities in the vicinity of the hole in the plane at $z = 0.18$ mm—the 3-D SFEM (left), the 2-D/1-D MSFEM without EE (middle), and the 2-D/1-D MSFEM with EE (right): x-components $\mathrm{Re}\{\boldsymbol{J}_x\}$ (above, ± 0.1 MA/m^2) and $\mathrm{Im}\{\boldsymbol{J}_x\}$ (below, $-3.0 - 0$ MA/m^2), $f = 1000$ Hz.

Further results with and without the EE, i.e., considering or neglecting the third term in (4), are presented below.

1) EE: Fig. 7 shows the EE by means of the z-component of the current density $\boldsymbol{J}$. For a fair comparison, the scaling of the colors is such that the corresponding figures use the same maximum and minimum. The ability to reproduce the EE by the 2-D/1-D MSFEM with EE is very good. A comparison of the x-component of the current densities with and without EE is shown in Fig. 8. It is easy to see that the method without EE completely fails. However, the new method with EE copes with the EE very well.

2) Planes of Symmetry: The plane $z = 0$ is always a plane of symmetry in the context of 2-D/1-D models considered by the MSFs. The present problem exhibits two additional planes of symmetry, $x = 0$ and $y = 0$, as shown in Fig. 9. Making use of them, only one quarter has to be simulated. Red boundary conditions are new or modified compared with the entire problem. Exploiting the symmetry works very well, as demonstrated in Fig. 9. Simulations have shown that the first three or four significant digits of the EC losses agree.

V. Higher Order 2-D/1-D MSFEM

Losses obtained by the 2-D/1-D MSFEMs have been compared with those by the 3-D SFEM in this section.

A. Linear 2-D/1-D MSFEM

There is a clear difference in the relative error of the losses between the 2-D/1-D MSFEMs with and without EE, i.e., with and without the third term in (4), as can be easily seen

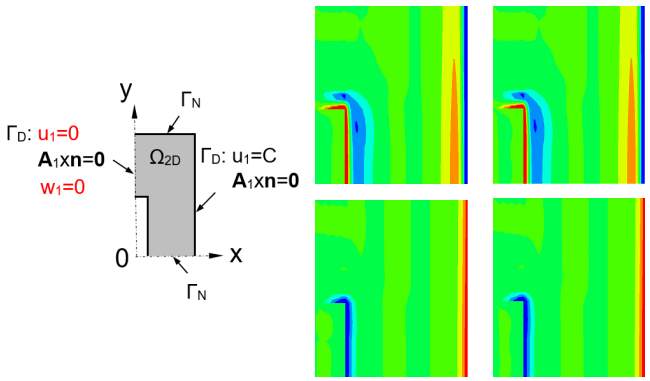

Fig. 9. Boundary conditions for u_1, $\boldsymbol{A}_1$, and w_1, $\Gamma_D \cup \Gamma_N = \partial\Omega_{2D}$; hole is included in $\Omega_{2D} = [0, 3] \times [0, 15]$ (left). Current densities in the vicinity of the hole at $z = 0.0$, 2-D/1-D MSFEM with EE, entire problem (middle), and one quarter (right): z-components $\mathrm{Re}\{\boldsymbol{J}_z\}$ (above, ± 0.1 MA/m^2) and $\mathrm{Im}\{\boldsymbol{J}_z\}$ (below, ± 2.0 MA/m^2), $f = 1000$ Hz.

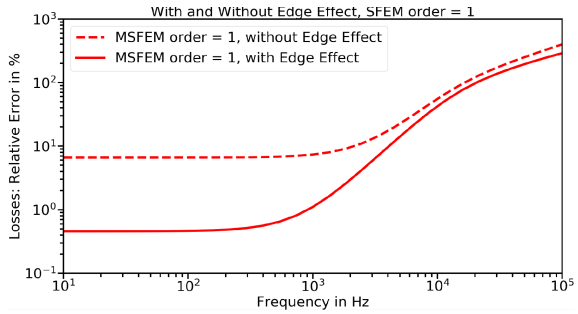

Fig. 10. Relative error of the EC losses versus the frequency of the linear 2-D/1-D MSFEMs with and without EE.

in Fig. 10. Both methods allow only a linear approximation. That is why the overall errors start to grow already at low frequencies due to the decreasing penetration depth.

B. Higher Order 2-D/1-D MSFEM Approach

To overcome the restriction to low frequencies in Section V-A, higher order odd terms (3rd and 5th) are added to the linear approach (4), leading to the higher order 2-D/1-D MSFEM approach

$$\begin{aligned}\tilde{\boldsymbol{A}} = {} & \phi_1^0(z)\,\mathrm{grad}(u_1(x, y)) \\ & + \phi_1(z)\boldsymbol{A}_1(x, y) + \mathrm{grad}(w_1(x, y)\phi_1(z)) \\ & + \phi_3(z)\boldsymbol{A}_3(x, y) + \mathrm{grad}(w_3(x, y)\phi_3(z)) \\ & + \phi_5(z)\boldsymbol{A}_5(x, y) + \mathrm{grad}(w_5(x, y)\phi_5(z)) + \cdots. \end{aligned} \tag{8}$$

The associated test function is constructed, and the weak form is derived analogously to the first-order 2-D/1-D MSFEMs (6) and (7), respectively. Higher order 2-D/1-D MSFEMs perform clearly better than the linear ones at higher frequencies, as demonstrated in Figs. 11 and 12. The higher the order, the better the 2-D/1-D MSFEMs perform. Consider that the EE provides essentially more accurate losses in a wide frequency range. The peak of the relative error in the third-order 2-D/1-D MSFEM occurs, because the sign changes at about 30 kHz. This would become visible using a linear scale for the relative error. The relative error of

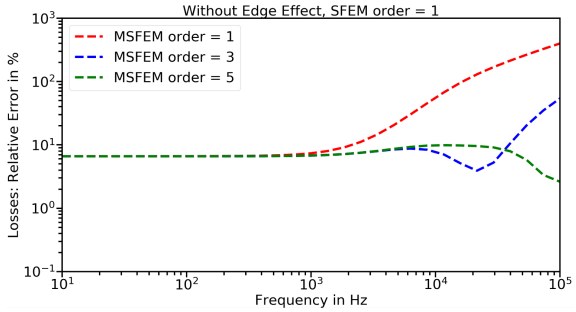

Fig. 11. Relative error of the EC losses versus the frequency of the higher order 2-D/1-D MSFEMs without EE.

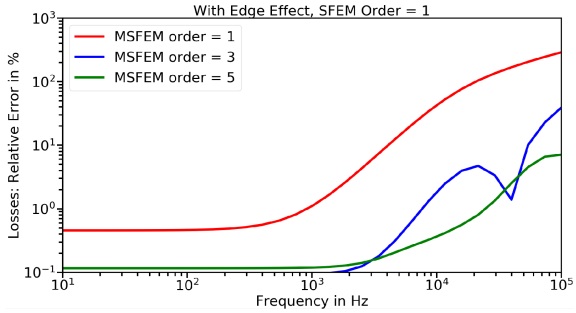

Fig. 12. Relative error of the EC losses versus the frequency of the higher order 2-D/1-D MSFEMs with EE.

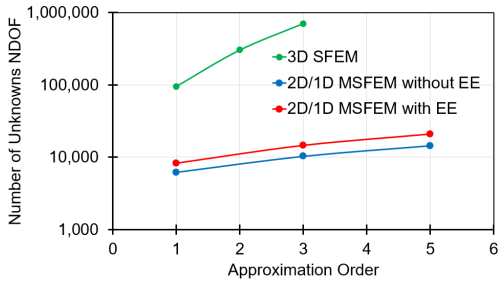

Fig. 13. Computational costs in terms of unknowns. The order of $\mathcal{U}_h$ and $\mathcal{V}_h$ were two and one, respectively, compared with (7).

the fifth-order 2-D/1-D MSFEM changes the sign above the observed frequency range.

C. Computational Costs

The NDOF is much smaller than that of the 3-D SFEM (see Fig. 13). Note that the coupling of the unknowns in the 3-D SFEM is much stronger too. The 3-D SFEM uses a mesh that is relatively fine to evaluate the relative errors in Sections V and VI accurately. Then NDOF can be reduced by the 2-D/1-D MSFEMs essentially.

VI. Conclusion

A new 2-D/1-D MSFEM, based on the MVP, has been presented, which is capable of considering both EE and air gaps between laminates. Increasing the order of the 2-D/1-D MSFEM copes very well with arbitrary penetration depths. Thanks to space splitting, the computational savings are enormous and the accuracy is excellent. The 2-D/1-D MSFEM can

obviously be extended to solve nonlinear problems, to this end, compared with [2] and [7].

ACKNOWLEDGMENT

This article was supported by the Austrian Science Fund (FWF) under projects P27028 and P31926.

REFERENCES

[1] P. Handgruber, A. Stermecki, O. Bíró, A. Belahcen, and E. Dlala, "Three-dimensional eddy-current analysis in steel laminations of electrical machines as a contribution for improved iron loss modeling," *IEEE Trans. Ind. Appl.*, vol. 49, no. 5, pp. 2044–2052, Sep./Oct. 2013.

[2] K. Hollaus and J. Schöberl, "Some 2-D multiscale finite-element formulations for the eddy current problem in iron laminates," *IEEE Trans. Magn.*, vol. 54, no. 4, Apr. 2018, Art. no. 7401716.

[3] O. Bottauscio, M. Chiampi, and D. Chiarabaglio, "Advanced model of laminated magnetic cores for two-dimensional field analysis," *IEEE Trans. Magn.*, vol. 36, no. 3, pp. 561–573, May 2000.

[4] J. Pippuri, A. Belahcen, E. Dlala, and A. Arkkio, "Inclusion of eddy currents in laminations in two-dimensional finite element analysis," *IEEE Trans. Magn.*, vol. 46, no. 8, pp. 2915–2918, Aug. 2010.

[5] O. Bottauscio and M. Chiampi, "Analysis of laminated cores through a directly coupled 2-D/1-D electromagnetic field formulation," *IEEE Trans. Magn.*, vol. 38, no. 5, pp. 2358–2360, Sep. 2002.

[6] P. Rasilo, E. Dlala, K. Fonteyn, J. Pippuri, A. Belahcen, and A. Arkkio, "Model of laminated ferromagnetic cores for loss prediction in electrical machines," *Electr. Power Appl.*, vol. 5, no. 7, pp. 580–588, Aug. 2011.

[7] M. Schöbinger, J. Schöberl, and K. Hollaus, "Multiscale FEM for the linear 2-D/1-D problem of eddy currents in thin iron sheets," *IEEE Trans. Magn.*, vol. 55, no. 1, Jan. 2019.

[8] O. Bottauscio, M. Chiampi, and D. Chiarabaglio, "Magnetic flux distribution and losses in narrow ferromagnetic strips," *J. Magn. Magn. Mater.*, vols. 215–216, pp. 46–48, Jun. 2000.

[9] M. Bali, H. De Gersem, and A. Muetze, "Finite-element modeling of magnetic material degradation due to punching," *IEEE Trans. Magn.*, vol. 50, no. 2, pp. 745–748, Feb. 2014.

[10] I. Babuska and J. M. Melenk, "The partition of unity method," *Int. J. Numer. Methods Eng.*, vol. 40, no. 4, pp. 727–758, Feb. 1997.